ACTA MECHANICA SINICA, Vol.19, No.5, October 2003 ISSN 0567-7718
The Chinese Society of Theoretical and Applied Mechanics
Chinese Journal of Mechanics Press, Beijing, China
Allerton Press, INC., New York, U.S.A.

LIFT AND POWER REQUIREMENTS OF HOVERING INSECT FLIGHT*

SUN Mao (孙 茂)† DU Gang (杜 刚)

(*Institute of Fluid Mechanics, Beijing University of Aeronautics & Astronautics, Beijing* 100083, *China*)

ABSTRACT: Lift and power requirements for hovering flight of eight species of insects are studied by solving the Navier-Stokes equation numerically. The solution provides velocity and pressure fields, from which unsteady aerodynamic forces and moments are obtained. The inertial torque of wing mass are computed analytically. The wing length of the insects ranges from 2 mm (fruit fly) to 52 mm (hawkmoth); Reynolds numbers Re (based on mean flapping speed and mean chord length) ranges from 75 to 3 850. The primary findings are shown in the following: (1) Either small ($R = 2$ mm, $Re = 75$), medium ($R \approx 10$ mm, $Re \approx 500$) or large ($R \approx 50$ mm, $Re \approx 4\,000$) insects mainly employ the same high-lift mechanism, delayed stall, to produce lift in hovering flight. The midstroke angle of attack needed to produce a mean lift equal to the insect weight is approximately in the range of 25° to 45°, which is approximately in agreement with observation. (2) For the small insect (fruit fly) and for the medium and large insects with relatively small wingbeat frequency (cranefly, ladybird and hawkmoth), the specific power ranges from 18 to 39 $W \cdot kg^{-1}$, the major part of the power is due to aerodynamic force, and the elastic storage of negative work does not change the specific power greatly. However for medium and large insects with relatively large wingbeat frequency (hoverfly, dronefly, honey bee and bumble bee), the specific power ranges from 39 to 61 $W \cdot kg^{-1}$, the major part of the power is due to wing inertia, and the elastic storage of negative work can decrease the specific power by approximately 33%. (3) For the case of power being mainly contributed by aerodynamic force (fruit fly, cranefly, ladybird and hawkmoth), the specific power is proportional to the product of the wingbeat frequency, the stroke amplitude, the wing length and the drag-to-lift ratio. For the case of power being mainly contributed by wing inertia (hoverfly, dronefly, honey bee and bumble bee), the specific power (without elastic storage) is proportional to the product of the cubic of wingbeat frequency, the square of the stroke amplitude, the square of the wing length and the ratio of wing mass to insect mass.

KEY WORDS: insects, hovering, unsteady aerodynamics, power requirement, computational fluid dynamics

1 INTRODUCTION

Recently, much progress has been made in revealing the unsteady high-lift mechanisms of insect flight. Since at the beginning of each down- or up-stroke, the wing of an insect was started at high angle of attack, dynamic stall was considered as a candidate for explaining the extra lift of insect wings. Dickinson and Götz[1] measured the aerodynamic forces of an airfoil started rapidly at high angles of attack in the Reynolds number (Re) range of fruit fly wing ($Re = 75 \sim 225$). They showed that lift was enhanced by the presence of a dynamic stall vortex, or leading edge vortex (LEV). After the initial start, lift coefficient as high as 2 was maintained within approximately 3 chord lengths of travel. Afterwards, lift drops due to the shedding of the LEV. For most insects, a section at $0.75R$ (R denotes the wing length) from the wing base travels approximately 5.5 chord lengths during a down- or up-stroke in hovering flight, which is much longer than 3 chord lengths (in forward flight, the section would travel an even larger distance during a down-stroke). Therefore, researchers assumed that dynamic stall was too short-lived to be

Revised 16 June, 2003
* The project supported by the National Natural Science Foundation of China (10232010)
† E-mail: sunmao@public.fhnet.cn.net

significant in flapping flight.

However, in 1996, Ellington and his colleagues[2,3] discovered that the LEV on the flapping wings (and model wings) of the hawkmoth *Manduca Sexta* did not shed in the translational phases of the down- and the up-strokes, or the delayed stall effect could be maintained in an entire stroke. They showed that a spanwise flow directed from wing-base to wing-tip existed on the flapping wing and suggested that the spanwise flow prevented the LEV from detaching. Analysis of the momentum in parted to fluid by the vortex wake showed that the LEV could produce enough lift for insect-weight support. This high-lift mechanism was termed delayed stall mechanism. for a flapping wing, Re is based on the mean chord length and the mean translational velocity at radius of the second moment of wing area, which is around $0.5 \sim 0.6R$ for most insects). Recently, Usherwood and Ellington[4,5] conducted force measurement on revolving real and model wings of various insects and a bird (quail), and for some cases, flow visualization was also conducted. They showed that the delayed stall mechanism (attachment of the LEV) exists for $Re = 600$ (mayfly) to 15 000 (quail) and for different wing planforms. Birch and Dickinson[6] measured the flows near and the aerodynamic forces on a model fruit fly wing in flapping motion ($Re = 100$). They also showed that the LEV did not shed in the translational phases of the down-stroke and the up-stroke and large life was maintained in these phases. These results show that the delayed stall mechanism is valid for most insects ($R = 2$ mm (fruit fly) to 50 mm (hawkmoth)). The delayed stall mechanism was confirmed by computational fluid dynamics (CFD) analyses[7~9].

Dickinson et al.[10] and Sane and Dickinson[11], by measuring the aerodynamic forces on a mechanical model of fruit fly wing in flapping motion, showed that when the translational velocity varied according to a trapezoidal function i.e. the translational velocity is constant throughout a stroke, punctuated by rapid accelerations at stroke reversal and the wing rotation was advanced (wing rotation proceeding the stroke reversal), in addition to the large lift during the translational phase of a down- or up-stroke, very large lift peaks occurred at the beginning and near the end of the strokes. Sun and Tang[12] and Ramamurti and Sandberg[13] simulated the flows of model fruit fly wings using CFD method, based on wing kinematics nearly identical to those used in the experiment of Dickinson et al.[10]. They obtained similar results as that of the experiment. The lift peak at the beginning of the stroke was attributed to the fast acceleration of the wing and the "wake capture" mechanism[12,14] and that near the end of the stroke to the wing rotation effects[10,12]. As a result of the above works and many others (see Refs. [15~25]), we are now able to understand how insects produce large lift better.

With the current understanding of the unsteady force production mechanisms, researchers have attempted to estimate the mechanical power of insect flight based on unsteady aerodynamic forces. Based on the measured unsteady drag on a model fruit fly wing in flapping motion, Sane and Dickinson[11] estimated that the mechanical power for a fruit fly might be considerably larger than the previous prediction by quasi-steady theory[26]. Sun and Tang[27], studied the lift and power requirements of hovering flight in the fruit fly by numerical simulation. Under the conditions where the mean lift balanced the insect weight, they computed the required mechanical power. With the computed mechanical power and available metabolic data, they obtained a value of 0.17 for the muscle efficiency, approximately twice as much as that estimated using the quasi-steady theory (0.09; Ref.[26]). Recently, Sun and Wu[28] have investigated the lift and power requirements in forward flight in a virtual fruit fly using CFD method.

In the above works on force balance and power requirements, only the small insect fruit fly was considered. It is of great interest to examine the same problems for various insects, and then to investigate the effects of morphological and kinematic parameters. In the present paper, we investigate the lift and power requirements of eight species of insects in hovering flight, for which detailed morphological and kinematic data are available[17,18,21,24,25]. These insects are as follows: four species from the order Diptera: fruit fly (FF) *Drosophila melanogaster*, cranefly (CF) *Tipula obsolete*, hoverfly (HF) *Episyrphas balteatus* and dronefly (DF) *Eristalis tenax*; one species from the order Coleoptera: ladybird (LB) *Coccinella 7-punctata*; two species from the order Hymenoptera: honey bee (HB) *Apis mellifera* and bumble bee (BB) *Bombus hortorum*. one species from the order Lepidoptera: hawkmoth (HM) *Manduca sexta*. The method of computational fluid dynamics is used in the study. In the method, the pressure and velocity fields around the flapping wing are obtained by solving the Navier-Stokes equations numerically; the lift and the torques due to the aerodynamic forces are calculated on the basis of the flow pressure and velocities. The inertial torques due to the accelera-

tion of the wing-mass is calculated analytically. From the aerodynamic and inertial torques, the mechanical power required for the flight is calculated.

2 COMPUTATIONAL METHOD

2.1 The Wing and the Coordinate Systems

The planforms of the wings of these insects are shown in Fig.1 (the planform of FF is from Zanker[29]; the rest are from Ellington[17]). The wing section is approximated by an ellipse of 12% thickness (the radius of the leading and trailing edges is only 0.2% of the chord length of the aerofoil). The radius of the second moment of wing area, denoted by r_2, is available and it ranges approximately from 0.5 to $0.6R$, where R is the wing length[17,21,25] (the mean flapping velocity at span location r_2 is used as reference velocity in the present study).

Two coordinate systems are used. One is inertial coordinate system, $OXYZ$; the origin O is at the wing base (see Fig.2), X and Y form the horizontal plane (X points backwards), and the Z-direction is vertical. The other is the body-fixed coordinate system $oxyz$. It has the same origin as the inertial coordinate system, but it rotates with the wing. The x axis is parallel to the wing chord and the y axis is on the pitching-rotation axis of the wing (see Fig.2).

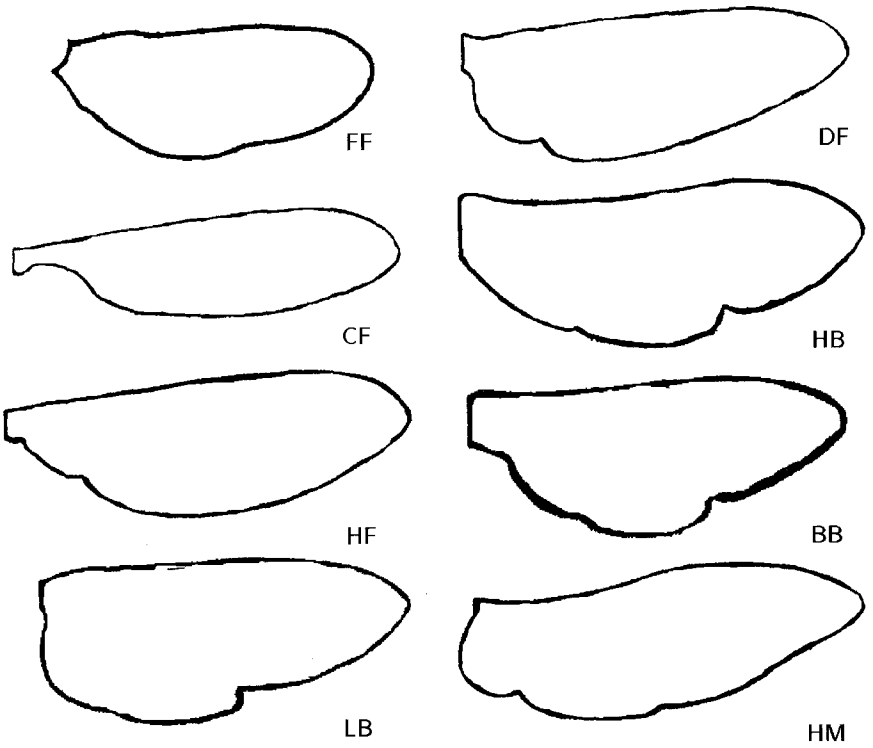

Fig.1 The wing planforms considered. FF, DF, CF, HF, LB, HB, BB and HM denote fruit fly, dronefly, cranefly, hoverfly, ladybird, bumble bee, honey bee and hawkmoth, respectively

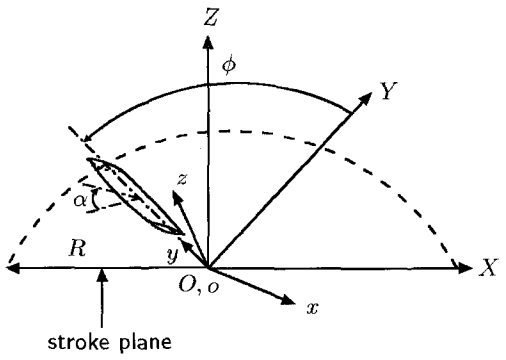

Fig.2 Sketches of the reference frames and wing motion

2.2 Governing Equation and Computation Method

The flow equations and computational method used in the present study are the same as these in Sun and Tang[12,27]. Only an outline of the method is given here. The Navier-Stokes equations are solved using the algorithm developed by Rogers and Kwak[30] and Rogers et al.[31], which is based on the method of artificial compressiblity. The algorithm uses a third-order flux-difference splitting technique for the convective terms and the second-order central difference for the viscous terms. The time derivatives in the momentum equation are differenced using a second-order, three-point, backward-difference formula. The algorithm is implicit and has second-order spatial and time accuracy.

2.3 Evaluation of the Aerodynamic Forces, Aerodynamic and Inertial Torques and Mechanical Power

Once the Navier-Stokes equations are numerically solved, the fluid velocity components and pressure at discretized grid points for each time step are available. The aerodynamic forces and torques acting on the wing are calculated from the pressure and the viscous stress on the wing surface. The inertial torques due to the acceleration of the wing-mass are calculated analytically.

The lift L is the component of the total aerodynamic force perpendicular to the translational velocity of the wing (defined below), i.e. perpendicular to the stroke plane, and is positive when it is in the positive Z direction (see Fig.2). The drag d is the component of the total aerodynamic force parallel to the translational velocity and is positive when directed opposite to the direction of the translational velocity of the down-stroke (the wing drag is the force that the insect must overcome for the translational motion of its wing and is relevant to the power requirement of flight). The coefficients of the above force components are defined as follows

$$C_L = \frac{L}{0.5\rho U^2 S} \tag{1}$$

$$C_d = \frac{d}{0.5\rho U^2 S} \tag{2}$$

where ρ is the fluid density, U is the reference velocity (defined below), and S is the wing area. The formulas for the aerodynamic and inertial torques and the mechanical power were given in Sun and Tang[27] and will not be repeated here.

2.4 Kinematics of the Flapping Wings

On the basis of the available kinematic data[18,21,22,24], the flapping motion is modeled as follows. The azimuthal rotation of the wing about the Z axis, which is normal to the stroke plane (see Fig.2), is called translation; the pitching rotation of the wing near the end of a stroke and at the beginning of the following stroke is called rotation or flip. The velocity at r_2, denoted by u_t, is called translational velocity and is approximated by the simple harmonic function

$$u_t^+ = 0.5\pi \sin(2\pi\tau/\tau_c) \tag{3}$$

where the non-dimensional translational speed of the wing $u_t^+ = u_t/U$ (U is the mean translational velocity of the wing over an up- or down-stroke and is used as reference velocity), $\tau = tU/c$ (t is dimensional time, c is the mean chord length of the wing and τ is the non-dimensional time), τ_c is the non-dimensional period of a flapping cycle. The azimuth-rotational speed of the wing is related to u_t. Denoting the azimuthal-rotational speed as $\dot{\phi}$, we have $\dot{\phi}(\tau) = u_t/r_2$. The geometric angle of attack of the wing is denoted by α. It takes a constant value except at the beginning or near the end of a stroke. The constant value is denoted by α_m, called as midstroke angle of attack. Here, we assume that the stroke plane is horizontal and α_m in the down-stroke is the same as that in the up-strokes. Around the stroke reversal, α changes with time and the angular velocity, $\dot{\alpha}$, is given by

$$\dot{\alpha}^+ = 0.5\dot{\alpha}_0^+\{1 - \cos[2\pi(\tau - \tau_r)/\Delta\tau_r]\}$$
$$\tau_r \le \tau \le (\tau_r + \Delta\tau_r) \tag{4}$$

where the non-dimensional form, $\dot{\alpha}^+ = \dot{\alpha}c/U$, $\dot{\alpha}_0^+$ is a constant, τ_r is the non-dimensional time at which the rotation starts (termed rotation timing), $\Delta\tau_r$ is the non-dimensional time interval over which the rotation lasts (termed rotation duration). In the time interval of $\Delta\tau_r$, the wing rotates from $\alpha = \alpha_m$ to $\alpha = 180° - \alpha_m$. Therefore, when α_m and $\dot{\alpha}_0^+$ are specified, $\Delta\tau_r$ can be determined. (Around the next stroke reversal, the wing would rotate from $\alpha = 180° - \alpha_m$ to $\alpha = \alpha_m$, the sign of the right-hand side of Eq.(4) should be reversed.) It is assumed that the axis of the pitching rotation is located at 30% of maximum chord length from the leading edge of the wing. On the basis of flight data[18,21,22,24], $\Delta\tau_r$ is approximately $0.25\tau_c$. These data also show that, in general, the wing rotation can be taken as symmetrical rotation, i.e. half the wing rotation is conducted near the end of a stroke and half at the beginning of the next stroke (as a result, τ_r may be determined from the value of $\Delta\tau_r$).

In the non-dimensional Navier-Stokes equations (non-dimensionalized by reference length c, reference velocity U and reference time c/U)[27], the only parameter needs to be specified is the Reynolds number Re. In the flapping motion discussed above, non-dimensional parameters need to be specified are τ_c (or the stroke amplitude Φ) and α_m (τ_c is related to Φ by $\tau_c = 2\Phi \cdot (r_2/R) \cdot (R/c)$). When a wing is given, its R, r_2/R, R/c, etc., are known. Thus, in calculating the aerodynamic force coefficients of the wing , we only need to specify Re, τ_c (or Φ) and α_m. Re and τ_c can be determined using available flight data. For most insects considered here, quantitative measurements of α_m do not exist. In the present study, α_m is so chosen such that the calculated mean lift balance the insect weight.

2.5 Data for Hovering Flight of the Insects

For FF, data of free hovering flight is not available, but data for very low speed flight (advance ratio is 0.16) have been given by Ennos[21]; these data are used here. For BB, data are taken from Dudley and Ellington[22]. For HM, data are taken from Willmott and Ellington[24,25]. For the rest five species, data are taken from Ellington[17,18]. The data include (see Table 1): insect mass m, mass of wing pair m_w, wing length R, the area of a single wing S, mean chord length c, second moment of wing area r_2, second moment of wing mass $r_{2,m}$, stroke amplitude Φ and stroke frequency n. Based on the wing mass and the second moment of wing mass, the moment of inertia of wing-mass, denoted by I (for one wing), is determined, the values of which are given in Table 1.

Table 1 Morphological and kinematic data of hovering flight

Species	m/mg	m_w/m/(%)	R/mm	c/mm	S/mm^2	r_2/R	$r_{2,m}/R$
Diptera: flies, mosquitoes							
Fruit fly (FF)	0.72	0.24*	2.02	0.67	1.36	0.596	0.48*
Cranefly (CF)	11.4	4.29	12.7	2.38	30.18	0.614	0.50
Hoverfly (HF)	27.3	1.27	9.3	2.20	20.48	0.578	0.44
Dronefly (DF)	68.4	1.50	11.4	3.19	36.89	0.543	0.40
Coleoptera: beetles							
Ladybird (LB)	34.4	2.87	11.2	3.23	36.12	0.538	0.40
Hymenoptera: bees							
Honey bee (HB)	101.9	0.50	9.8	3.08	30.14	0.566	0.45
Bumble bee (BB)	175	0.52	13.2	4.02	54.9	0.554	0.46
Lepidoptera: moths							
Hawkmoth (HM)	1648	5.79	51.9	18.26	947.8	0.525	0.38

Species	Φ/(°)	n/(s^{-1})	I/(g·cm^2)	U/(cm·s^{-1})	Re	τ_c	$\bar{C}_{L,W}$
Diptera: flies, mosquitoes							
Fruit fly (FF)	150	254	0.80×10^{-8}	160	75	9.38	1.59
Cranefly (CF)	123	45.5	0.95×10^{-4}	152	251	14.09	1.26
Hoverfly (HF)	90	160	0.25×10^{-4}	268	413	7.54	1.48
Dronefly (DF)	109	157	0.11×10^{-3}	370	832	7.27	1.05
Coleoptera: beetles							
Ladybird (LB)	177	54	0.95×10^{-4}	201	450	11.54	1.82
Hymenoptera: bees							
Honey bee (HB)	131	197	0.50×10^{-4}	500	1067	8.25	1.08
Bumble bee (BB)	116	155	0.17×10^{-3}	459	1326	7.12	1.17
Lepidoptera: moths							
Hawkmoth (HM)	121	26.3	0.184	304	3852	6.32	1.5

* m_w/m and $r_{2,m}/R$ for D. melanogaster are not available; the values shown are that of D. virilis

From the above data, the mean translational velocity of the wing $U(= 2n\Phi r_2)$ is computed first. Then Re and τ_c are calculated as follows: $Re = cU/\nu$ (where $\nu = 0.144\,\mathrm{cm}^2/\mathrm{s}$); $\tau_c = (1/n)/(U/c)$. The mean lift coefficient required for weight support $\bar{C}_{L,W}$ is computed as $\bar{C}_{L,W} = mg/\rho U^2 S$ (where $g = 981\,\mathrm{cm/s}^2$, $\rho = 1.25 \times 10^{-3}\,\mathrm{g/cm}^3$). The results are also given in Table 1.

3 RESULTS AND DISCUSSION

3.1 Validation

The code used here is the same as that in Sun and Tang[27]. It is based on the flow computation method outlined above, and was developed by Lan

and Sun[9]. It was verified by the analytical solutions of simple flows (boundary layer flow on a flat plate[9]; flow at the beginning of a suddenly started aerofoil[32]) and tested by measured steady-state pressure distributions on a wing[9].

Recently, the code was further tested[27,28] by measured unsteady aerodynamic forces on a model fruit fly wing in flapping motion. The calculated drag coefficient agrees well with the measured (see Fig.2(A) and Fig.2(C) of Sun and Wu[28]). For the lift coefficient (see Fig.2(B) and Fig.2(D) of Sun and Wu[28] and Fig.4 of Sun and Tang[27]), in the translational phase of the down-stroke, the computed value agrees well with the measured; around the stroke reversal, the computed peak values are smaller than the measured; in the translational phase of the up-stroke, the computed value is a little less than the measured, but they are in qualitative agreement (note that the value of the measured lift coefficient in the up-stroke is higher than that in the down-stroke). These comparisons show that although the CFD simulations might not accurately capture all the flow features around the stroke reversal, the agreement of the aerodynamic force coefficients between the computational and experimental simulations is reasonably good. We think that the present CFD method can calculate the unsteady aerodynamic forces and torques of the model insect wing with reasonable accuracy.

Grids used in the following computation have dimensions $100 \times 109 \times 105$ in normal direction, around the wing section and in spanwise direction, respectively; the normal grid spacing at the wall is $0.001\,5c$ and the outer boundary is at $20c$ from the wing; the non-dimensional time step is 0.02. As an example, a portion of the grid used for the bumble bee wing is shown in Fig.3.

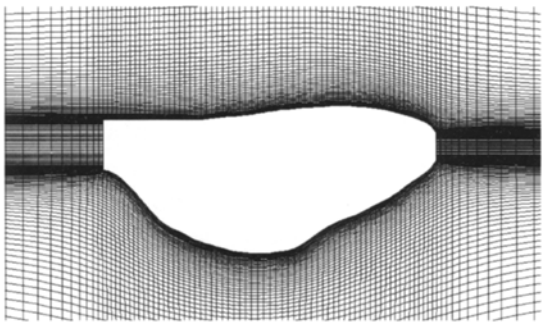

Fig.3 Portions of the grid for the bumble bee wing

3.2 Force Balance in Hovering Flight

Since we wished to study the aerodynamic force and power requirements for balanced flight, we first investigated the force balance. For the insects considered here, the stroke plane is approximately horizontal[18,21,24]; as a result, the mean thrust on the wing over each flapping cycle is zero and the horizontal force is automatically balanced. Thus we only need to consider under what conditions the weight of the insect is balanced by the mean lift.

As noted above, the non-dimensional parameters required in the calculation of the aerodynamic force coefficients are Re, τ_c and α_m. Of them, Re and τ_c have been determined above using the flight data (Table 1). α_m is determined using the force balance condition as follow: a value of α_m is guessed; the flow equations are solved and the corresponding mean lift $\bar{C}_L$ is calculated; $\bar{C}_L$ is compared with $\bar{C}_{L,\mathrm{W}}$; if $\bar{C}_L$ is not equal to $\bar{C}_{L,\mathrm{W}}$, α_m is adjusted; the calculation is repeated until the difference between $\bar{C}_L$ and $\bar{C}_{L,\mathrm{W}}$ is less than 0.03.

The calculated α_m and $\bar{C}_L$ are shown in Table 2. For CF, HF, DF, HB, BB and LB, Ellington[18]

Table 2 Calculated results

Species	$\alpha_m/(^\circ)$	$\bar{C}_L$	$\bar{C}_d$	$C^+_{\mathrm{W,t}}$	$C^-_{\mathrm{W,t}}$	$(P^*)_1/(\mathrm{W\cdot kg^{-1}})$	$(P^*)_2/(\mathrm{W\cdot kg^{-1}})$
Diptera: flies, moquitors							
Fruit fly (FF)	46	1.59	2.11	14.15	−0.212	30	30
Cranefly (CF)	30	1.29	1.02	11.24	−1.77	18	16
Hoverfly (HF)	29	1.46	0.78	16.24	−4.87	39	27
Dronefly (DF)	26	1.06	0.76	6.60	−3.19	62	32
Coleoptera: beetles							
Ladybird (LB)	43	1.81	1.75	16.27	−1.43	31	28
Hymenoptera: bees							
Honey bee (HB)	25	1.08	0.89	5.49	−1.77	61	41
Bumble bee (BB)	28	1.17	0.95	5.17	−1.27	56	42
Lepidoptera: moths							
Hawkmoth (HM)	32	1.50	0.88	13.37	−2.94	42	33

observed that α_m is typically 35°; the presented calculation gives values ranging from 23° (DF) to 43° (LB). Vogel[33] measured the angle of attack for tethered *Drosophila Virilis* flying in still air; α_m is approximately 45°; our calculated value for FF (*D. melanogaster*) is 46°. For HW, Willmott and Ellington[24] observed that $\alpha_m \approx 40°$, the calculated values are 32°. The above computated results are in reasonably good agreement with observation.

3.3 The Mechanism of Aerodynamic Force Generation

The mean force coefficients are computed from the time courses of the force coefficients in one flapping cycle. The time courses of C_L and C_d in one cycle are plotted in Fig.4 and Fig.5. As seen in Fig.4(b) and Fig.5(b), the major part of the mean lift comes from the mid-portions of the down- and up-strokes and the contribution from wing rotation around stroke reversal is relatively small. As discussed in Dickinson et al.[10] and Sun and Tang[12], the large C_L in the mid-portion of a down- or up-stroke, during which the wing is in pure translational motion, is due to the delayed stall mechanism. According to Fig.4 and Fig.5,

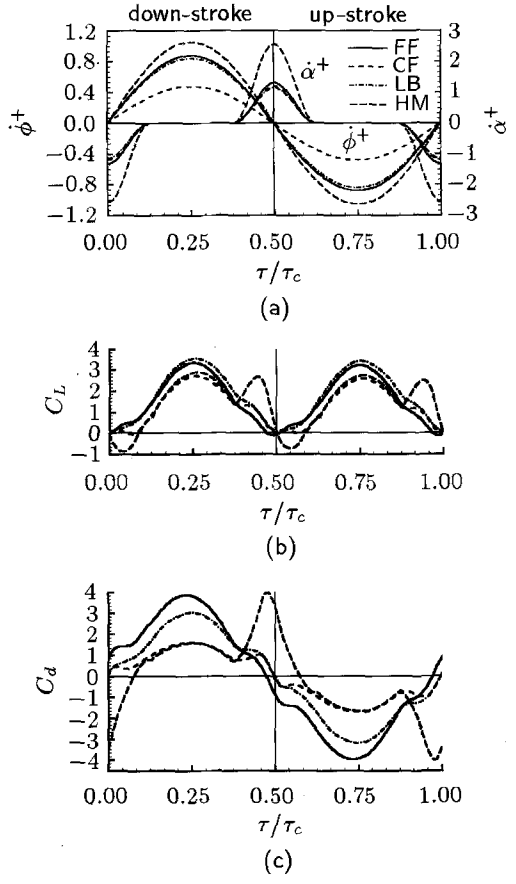

Fig.4 Lift and drag coefficients vs. time in one cycle (FF, CF, LB and HM)

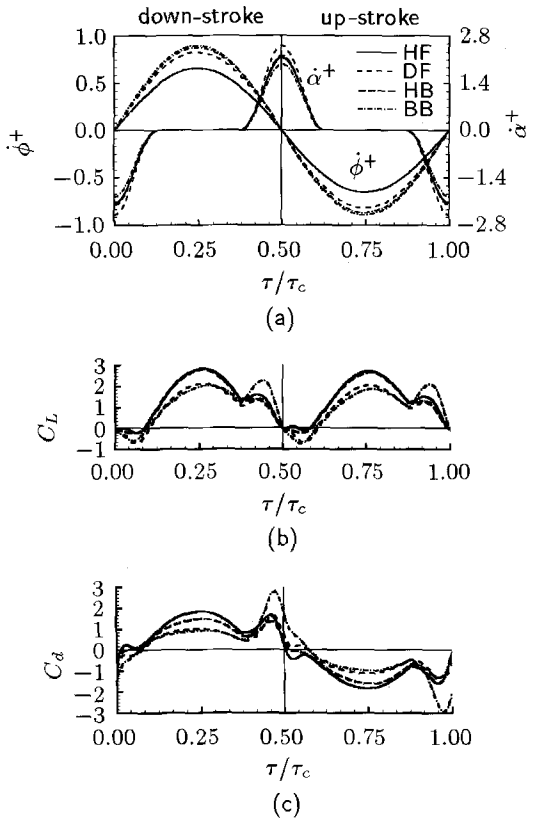

Fig.5 Lift and drag coefficients vs. time in one cycle (HF, DF, HB, BB)

it is estimated that around 80% of the mean lift comes from pure translational motion, or is due to the delayed stall mechanism. Figure 6 shows the vorticity plots at the end of the translational phase for all insects considered. It is seen that for all the insects, the LEV does not shed in the translational phase; when Re is larger, the LEV is more concentrated. Results here suggest that either small ($R = 2\,\text{mm}$, $Re = 75$), medium ($R \approx 10\,\text{mm}$, $Re \approx 500$) or large ($R \approx 50\,\text{mm}$, $Re \approx 4\,000$) insects mainly employ the same high-lift mechanism, delayed stall, in hovering flight. (Recent experiments on revolving model wings of various insects[4,5] and revolving model fruit fly wing[10] have also shown that the delayed stall mechanism exists for a wide Reynolds number range, $Re \approx 100 \sim 15\,000$.)

3.4 Power Requirements

As shown above, at some α_m (ranging from 23° to 46°), an insect of the eight species considered can produce enough lift to support its weight and the lift is mainly due to the delayed stall mechanism. Note that when generating large lift, the delayed stall mechanism also produces large drag (see Table 2 and Fig.4(c) and Fig.5(c)). In the following, we calculated the power required to maintain this lift and investigated the mechanical power output during hovering

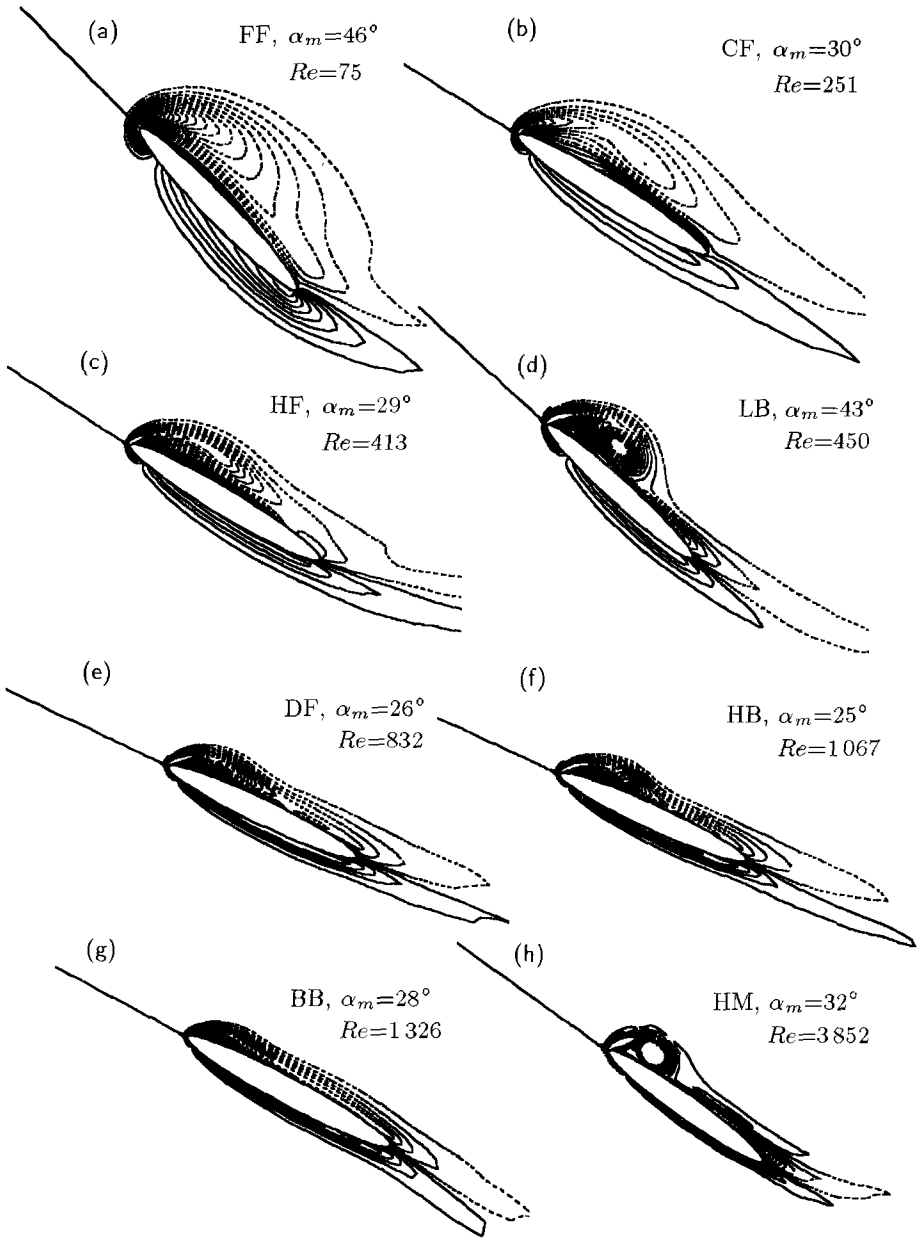

Fig.6 Vorticity plots at half-wing length near the end of the down-stroke (α_m, angle of attack of wing). Solid and broken lines indicate positive and negative vorticity, respectively. The magnitude of the non-dimensional vorticity at the outer contour is 1 and the contour interval is 3

flight.

As expressed in Eq.(20) of Sun and Tang[27], the aerodynamic power is consisted of two parts, one due to the aerodynamic torque for translation and the other to the aerodynamic torque for rotation. The coefficients of these two torques, denoted as $C_{\mathrm{Q,a,t}}$ and $C_{\mathrm{Q,a,r}}$, respectively, are shown in Fig.7 for the bumble bee. It is seen that $C_{\mathrm{Q,a,t}}$ is much larger than $C_{\mathrm{Q,a,r}}$. This is true for other insects considered.

The inertial power is also consisted of two parts (see Eq.(35) of Sun and Tang[27]), one due to the inertial torque for translation and the other to the inertial torque for rotation. The inertial torque for rotation can not be calculated since the moment of inertia of the wing-mass about the axis of flip rotation is not available. Because most of the wing-mass is located near the axis of flip rotation, it is expected that the inertial torque for rotation is much smaller than that for translation. That is, both the aerodynamic and inertial torques for rotation might be much smaller than those for translation. In the present work, the aerodynamic and inertial torques for rotation are ne-

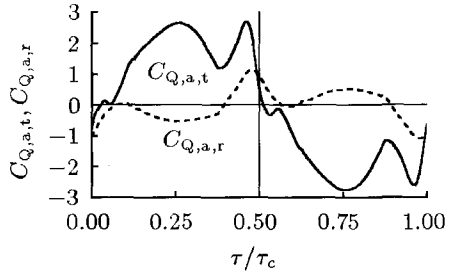

Fig.7 Aerodynamic torque coefficients for translation and for rotation vs. time in one cycle (BB)

glected in the power calculation.

The coefficients of aerodynamic ($C_{Q,a,t}$) and inertial ($C_{Q,i,t}$) torques for translation are shown in Fig.8 and Fig.9 for the eight species of insects. The

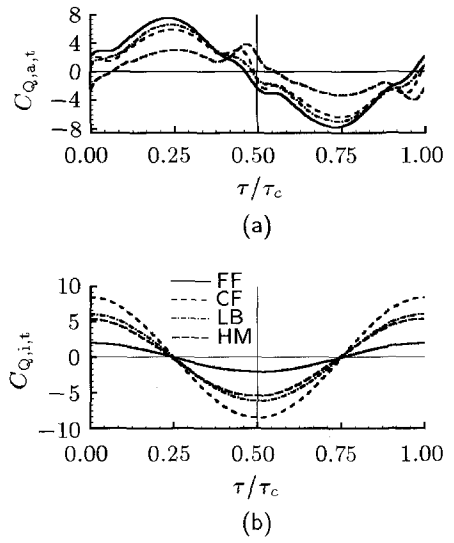

Fig.8 Aerodynamic and inertial torque coefficients vs. time in one cycle (FF, CF, LB, HM)

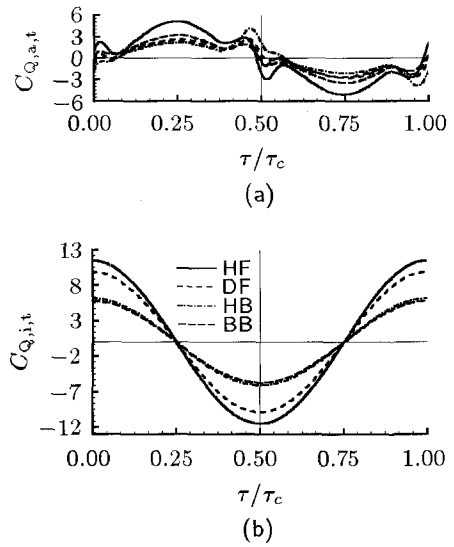

Fig.9 Aerodynamic and inertial torque coefficients vs. time in one cycle (HF, DF, HB, BB)

$C_{Q,a,t}$ curves are similar to the corresponding C_d curves for obvious reasons. With $C_{Q,a,t}$ and $C_{Q,i,t}$, the power coefficient (C_P) can be computed using Eqs.(41)~(43) of Sun and Tang[27]. C_P for the eight species are shown in Fig.10. In the figure, contributions by the aerodynamic and inertial torques (denoted by $C_{P,a}$ and $C_{P,i}$, respectively) are also shown (C_P is the sum of $C_{P,a}$ and $C_{P,i}$). C_P is positive for the early (relatively large) part of a down- or up-stroke and negative for the later (relatively small) part of the stroke. Apparently, the negative power is due to the inertial torque in the second half of the down- or up-stroke. It is interesting to note that the time course of C_P is similar to that of $C_{P,a}$ for FF, CF, LB and HM, but to that of $C_{P,i}$ for HF, DF, HB and BB; i.e. the aerodynamic power is much larger than the inertial power for the former four species and the opposite is true for the latter four species. Some explanations are given below. From Eqs.(15) and (33) of Sun and Tang[27], the inertial and aerodynamic torques (denoted by $Q_{i,t}$ and $Q_{a,t}$, respectively) can be written as

$$Q_{i,t} \sim I\Phi n^2 = 0.5 m_w \hat{r}_{2,m}^2 R^2 \Phi n^2 \tag{5}$$

$$Q_{a,t} \sim \hat{r}_d \frac{\bar{C}_d}{\bar{C}_{L,W}} mR \approx \hat{r}_d \frac{\bar{C}_d}{\bar{C}_L} mR \tag{6}$$

where m_w is the wing mass (two wings), $\hat{r}_{2,m}$ is the radius of the second moment of wing mass normalized by R, $\bar{C}_d$ is the mean drag coefficient and $\hat{r}_d$ is the radius of the first moment of wing drag normalized by R. Equations.(5) and (6) give

$$Q_{i,t}/Q_{a,t} \sim \frac{m_w}{m} \frac{\hat{r}_{2,m}^2}{\hat{r}_d} \frac{\bar{C}_L}{\bar{C}_d} \Phi R n^2 \tag{7}$$

If it is assumed that $\hat{r}_{2,m}^2$, $\hat{r}_d$ and Φ do not vary greatly from one insect to another, we have

$$Q_{i,t}/Q_{a,t} \sim \bar{C}_L/\bar{C}_d \cdot \frac{m_w}{m} R n^2 \tag{8}$$

For FF, although n is large, yet R is very small (in addition, its $\bar{C}_L/\bar{C}_d$, as seen in Table 2, is very small), thus the inertial torque is small compared to the aerodynamic torque, resulting in the small inertial power compared to aerodynamic power. For CF, LB and HM, n is relatively small; thus the inertial torque is small compared to the aerodynamic torque, again resulting in the small inertial power compared to the aerodynamic power. We can explain the large inertial power (compared to aerodynamic power) for HF, DF, HB and BB by similar reasoning.

Integrating C_P over the part of a wingbeat cycle where it is positive gives the coefficient of positive

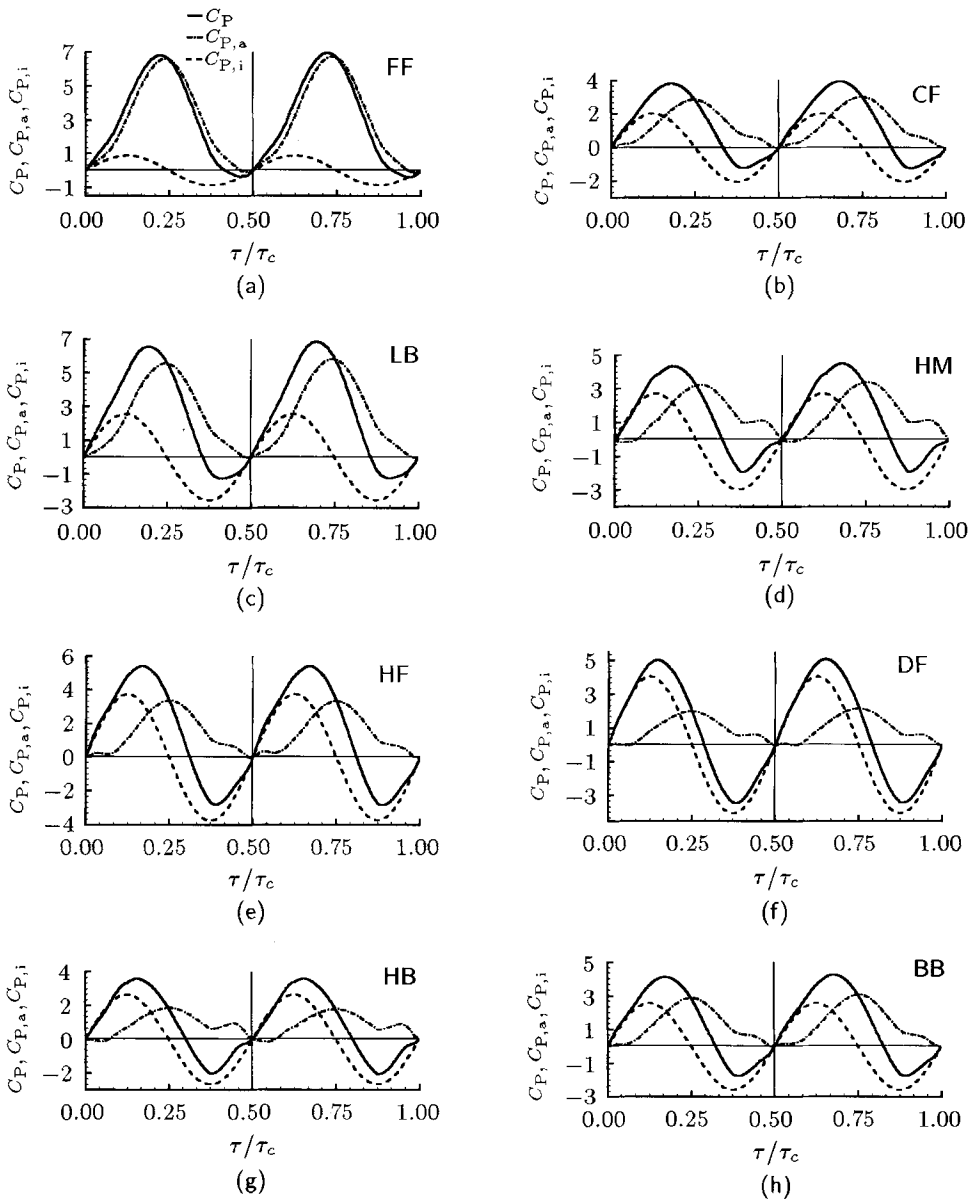

Fig.10 Coefficients of power for translation vs. time in one cycle. C_P, coefficient of power; $C_{P,a}$, contribution by aerodynamic force; $C_{P,i}$, contribution by inertial force

work for translation, which is represented by $C^+_{W,t}$. Integrating C_P over the part of the cycle where it is negative gives the coefficient of "negative" work for "braking" the wing in this part of the cycle, which is represented by $C^-_{W,t}$. The results of the integration for the insects are shown in Table 2 (for FF, CF, LB and HM, $C^-_{W,t}$, the negative work is much smaller then $C^+_{W,t}$, the positive work).

The mass specific power, repressed by P^*, is defined as the mean mechanical power over a flapping cycle divided by the mass of the insect, and it can be written as follows

$$P^* = 0.5\rho U^3 \times (2S) \times (C_W/\tau_c)/m$$
$$= (981) \times UC_W/(\tau_c \times \bar{C}_{L,G}) \quad (9)$$

where C_W is the coefficient of work per cycle[27]. When calculating C_W, one needs to consider how the negative work fits into the power budget[20]. There are three possibilities[20,34]. One is that the negative power is simply dissipated as heat and sound by some form of an end stop, then it can be ignored in the power budget. The second is that in the period of negative work, the excess energy can be stored by an elastic element, and this energy can then be released when the wing does positive work. The third is that the flight muscles do negative work (i.e. they are stretched while developing tension, instead of contracting as in "positive" work) but the negative work uses much less metabolic energy than an equiva-

lent amount of positive work, and again, the negative power can be ignored in the power budget. That is, out of these three possibilities, two ways of computing C_{W} can be taken. One is neglecting the negative work, i.e.

$$C_{\mathrm{W}} = C^{+}_{\mathrm{W,t}} \tag{10}$$

The other is assuming the negative work can be stored and released when the wing does positive work, i.e.

$$C_{\mathrm{W}} = C^{+}_{\mathrm{W,t}} - |C^{-}_{\mathrm{W,t}}| = C^{+}_{\mathrm{W,t}} + C^{-}_{\mathrm{W,t}} \tag{11}$$

With C_{W} computed by Eq.(10) or Eq.(11), the specific power P^* can be computed using Eq.(9). When C_{W} is computed by Eq.(10), the resulting P^* is denoted by $(P^*)_1$; when C_{W} is computed by Eq.(11), the resulting P^* is denoted by $(P^*)_2$. The results are given in Table 2. When elastic storage of negative power is not considered, for fruit fly, cranefly, ladybird and hawkmoth, the specific power is in the range of 18 to 39 $\mathrm{W{\cdot}kg^{-1}}$, while for dronefly, hoverfly, honeybee and bumblebee, the specific power is much higher, ranging from 39 to 61 $\mathrm{W{\cdot}kg^{-1}}$. When elastic power storage of negative power is considered, for the former four insects, P^* ranges from 16 to 33 $\mathrm{W{\cdot}kg^{-1}}$ and for the later four insects, P^* ranges from 27 to 42 $\mathrm{W{\cdot}kg^{-1}}$.

The above results show that for small insect like fruit fly ($R = 2\,\mathrm{mm}$) and for medium ($R \approx 10\,\mathrm{mm}$) and large ($R \approx 50\,\mathrm{mm}$) insects with n relatively small (CF, LB and HM), because the inertial power is small compared to the aerodynamic power, elastic storage of negative work does not change the specific power greatly; while for medium and large insects with n relatively large (HF, DF, HB and BB), because the inertial power is large compared to the aerodynamic power, the elastic storage of negative power can decrease the specific power significantly.

Finally, we have some more discussion on how the morphological and kinematic parameters influence P^*. As mentioned above, for FF, CF, LB and HM, P^* (without elastic storage) ranges from 18 to 39 $\mathrm{W{\cdot}kg^{-1}}$. For these four insects, the majority of the power is due to aerodynamic torque and from Eq.(6), P^* can be written as

$$P^* \sim \hat{r}_d n \Phi R \frac{\bar{C}_d}{\bar{C}_L} \tag{12}$$

As an example, we consider the LB ($P^* = 31\,\mathrm{W{\cdot}kg^{-1}}$) and the CF ($P^* = 18\,\mathrm{W{\cdot}kg^{-1}}$). They have about the same R (and S). But the ladybird has larger Φ and n (because its weight is much larger) and its $\bar{C}_d/\bar{C}_L$ is also larger (because its wings operate at higher α_m), resulting the larger P^*. Examination of the data in Tables 1 and 2 shows that the calculated P^* for the above four insects varies with n, Φ, R and $\bar{C}_d/\bar{C}_L$ approximately according to Eq.(12).

For HF, DF, HB and BB, P^* (without elastic storage) ranges from 39 to 61 $\mathrm{W{\cdot}kg^{-1}}$. For these four insects (R medium or large, n relatively large), the majority of power is due to inertial torque and from Eq.(5), P^* can be written as

$$P^* \sim \hat{r}^2_{2,m} \frac{m_{\mathrm{w}}}{m} n^3 \Phi^2 R^2 \tag{13}$$

Again, examination of the data in Tables 1 shows that P^* for these four insects varies with n, Φ, R and m_{w}/m approximately according to Eq.(13).

These results suggest that for small insect like fruit fly and for medium and large insects with relatively small n, P^* (mainly due to aerodynamic force) is proportional to the product of n, Φ, R and $\bar{C}_d/\bar{C}_L$, and that for medium and large insects with relatively large n, P^* (mainly due to wing inertia) is proportional to the product of n^3, Φ^2, R^2 and m_{w}/m.

4 CONCLUSIONS

(1) Either small ($R = 2\,\mathrm{mm}$, $Re = 75$), medium ($R \approx 10\,\mathrm{mm}$, $Re \approx 500$) or large ($R \approx 50\,\mathrm{mm}$, $Re \approx 4\,000$) insects mainly employ the same high-lift mechanism, delayed stall, to produce lift in hovering flight. The midstroke angle of attack needed to produce a mean lift equal to the insect weight is approximately in the range of 25° to 45° which is in agreement with observation.

(2) For the small insect (fruit fly) and for the medium and large insects with relatively small wingbeat frequency (cranefly, ladybird and hawkmoth), the specific power ranges from 18 to 39 $\mathrm{W{\cdot}kg^{-1}}$, the major part of the power is due to aerodynamic force, and the elastic storage of negative work does not change the specific power greatly. However, for medium and large insects with relatively large wingbeat frequency (hoverfly, dronefly, honey bee and bumble bee), the specific power ranges from 39 to 61 $\mathrm{W{\cdot}kg^{-1}}$, the major part of the power is due to wing inertia, and the elastic storage of negative work can decrease the specific power by approximately 33%.

(3) For the case of power being mainly contributed by aerodynamic force (fruit fly, cranefly, ladybird and hawkmoth), the specific power is proportional to the product of the wingbeat frequency, the stroke amplitude, the wing length and the drag-to-lift ratio. For the case of power being mainly contributed by wing inertia (hoverfly, dronefly, honey

bee and bumble bee), the specific power (without elastic storage) is proportional to the product of the cubic of wingbeat frequency, the square of the stroke amplitude, the square of the wing length and the ratio of wing mass to insect mass.

REFERENCES

1 Dickinson MH, Götz KG. Unsteady aerodynamic performance of model wings at low Reynolds numbers. *J Exp Biol*, 1993, 174: 45~64

2 Ellington CP, van den Berg C, Willmott AP. Leading edge vortices in insect flight. *Nature*, 1996, 384: 626~630

3 Willmott AP, Ellington CP, Thomas AR. Flow visualization and unsteady aerodynamics in the flight of the hawkmoth, Manduca sexta. *Trans R Soc Lond*, 1997b, 352: 303~316

4 Usherwood JR, Ellington CP. The aerodynamics of revolving wings. I. Model hawkmoth wings. *J Exp Biol*, 2002, 205: 1547~1564

5 Usherwood JR, Ellington CP. The aerodynamics of revolving wings. II. Propeller force coefficients from mayfly to quail. *J Exp Biol*, 2002, 205: 1565~1576

6 Birch JM, Dickinson MH. Spanwise flow and the attachment of the leading-edge vortex on insect wings. *Nature*, 2001, 412: 729~733

7 Liu H, Ellington CP, Kawachi K, et al. A computational fluid dynamic study of hawkmoth hovering. *J Exp Biol*, 1998, 201: 461~477

8 Wang ZJ. Two dimensional mechanism for insect hovering. *Phys Rev Lett*, 2000, 85: 2216~2219

9 Lan SL, Sun M. Aerodynamic of properties of a wing performing unsteady rotational motions at low Reynolds number. *Acta Mech*, 2001, 149: 135~147

10 Dickinson MH, Lehman FO, Sane SP. Wing rotation and the aerodynamic basis of insect flight. *Science*, 1999, 284: 1954~1960

11 Sane SP, Dickinson MH. The control of flight force by a flapping wing: lift and drag production. *J Exp Biol*, 2001, 204: 2607~2626

12 Sun M, Tang J. Unsteady aerodynamic force generation by a model fruit fly wing in flapping motion. *J Exp Biol*, 2002, 205: 55~70

13 Ramamurit R, Sandberg WC. A three-dimensional computational study of the aerodynamic mechanisms of insect flight. *J Exp Biol*, 2002, 205: 1507~1518

14 Birch JM, Dickinson MH. The influence of wing-wake interactions on the production of aerodynamic forces in flapping flight. *J Exp Biol*, 2003, 206: 2257~2272

15 Vogel S. Flight in Drosophila. I. Flight performance of tethered flies. *J Exp Biol*, 1966, 44: 567~578

16 Weis-Fogh T. Quick estimates of flight fitness in hovering animals, including novel mechanism for lift production. *J Exp Biol*, 1973, 59: 169~230

17 Ellington CP. The aerodynamics of hovering insect flight. II. Morphological parameters. *Phil Trans R Soc Lond*, B, 1984, 305: 17~40

18 Ellington CP. The aerodynamics of hovering insect flight. III. Kinematics. *Phil Trans R Soc Lond*, B, 1984, 305: 41~78

19 Ellington CP. The aerodynamics of hovering insect flight. IV. Aerodynamic mechanisms. *Phil Trans R Soc Lond*, B, 1984, 305: 79~113

20 Ellington CP. The aerodynamics of hovering insect flight. VI. Lift and power requirements. *Phil Trans R Soc Lond*, B, 1984, 305: 145~181

21 Ennos AR. The kinematics and aerodynamics of the free flight of sôme Diptera. *J Exp Biol*, 1989, 142: 49~85

22 Dudley R, Ellington CP. Mechanics of forward flight in bumblebees. I. Kinematics and morphology. *J Exp Biol*, 1990a, 148: 19~52

23 Dudley R, Ellington CP. Mechanics of forward flight in bumblebees. II. Quasi-steady lift and power requirements. *J Exp Biol*, 1990b, 148: 53~88

24 Willmott AP, Ellington CP. The mechanics of flight in the hawkmoth Manduca sexta. I. Kinematics of hovering and forward flight. *J Exp Biol*, 1997, 200: 2705~2722

25 Willmott AP, Ellington CP. The mechanics of flight in the hawkmoth Manduca sexta. II. Aerodynamic consequences of kinematic and morphological variation. *J Exp Biol*, 1997b, 200: 2723~2745

26 Lehman FO, Dickinson HD. The changes in power requirements and muscle efficiency during elevated force production in the fruit fly Drosophila melanogaster. *J Exp Biol*, 1997, 200: 1133~1143

27 Sun M, Tang J. Lift and power requirements of hovering flight in Drosophila virilis. *J Exp Biol*, 2002, 205: 2413~2427

28 Sun M, Wu JH. Lift generation and power requirements of fruit fly in forward flight with modeled wing motion. *J Exp Biol*, 2003, 206: 3065~3083

29 Zanker JM. The wing beat of Drosophila melanogaster. I. Kinematics. *Phil Trans R Soc Lond*, B, 1990, 327: 1~18

30 Rogers SE, Kwak D. Upwind differencing scheme for the time-accurate incompressible Navier-Stokes equations. *AIAA J*, 1990, 28: 253~262

31 Rogers SE, Kwak D, Kiris C. Steady and unsteady solutions of the incompressible Navier-Stokes equations. *AIAA J*, 1991, 29: 603~610

32 Lan SL, Sun M. Aerodynamic interaction between two airfiols in unsteady motions. *Acta Mech*, 2001, 150: 39~51

33 Vogel S. Flight in Drosophila. II. Variations in stroke parameters and wing contour. *J Exp Biol*, 1967, 46: 383~392

34 Weis-Fogh T. Energetics of hovering flight in hummingbirds and in Drosophila. *J Exp Biol*, 1972, 56: 79~104